ACS OMEGA

Open Access

http://pubs.acs.org/journal/acsodf

Article

Preparation of Red-Emitting CDs for Glioma Imaging and Fe^{3+} Sensing

Shiqiang Hou, Ning Lin,* and Yi Wang*

Cite This: *ACS Omega* 2024, 9, 44418−44424

Read Online

ACCESS | Metrics & More | Article Recommendations | Supporting Information

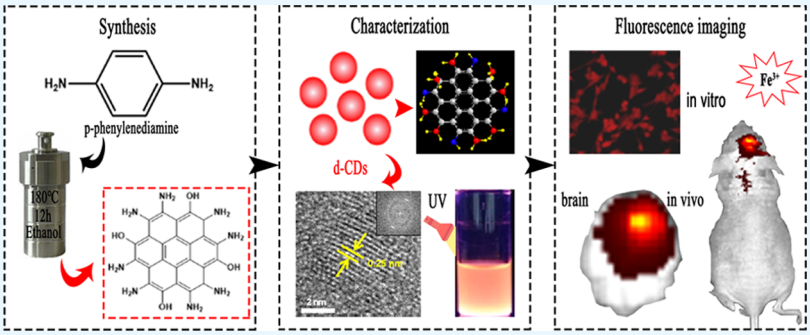

ABSTRACT: Red-emitting fluorescent carbon dots (CDs) have garnered significant attention due to their wide-ranging applications in biological fields. However, challenges such as complex precursors, labor-intensive preparation processes, and low quantum yields have hindered their broader utilization. In this study, we developed a simple and efficient solvothermal method to synthesize fluorescent CDs with tunable emission wavelengths using aniline derivatives as precursors. The emission wavelengths of the synthesized CDs were influenced by the functional groups at the *para*-position of the aniline derivatives with stronger electron-donating effects leading to a red shift in emissions. Notably, bright red-emitting CDs with a quantum yield of 19.42% and excellent photobleaching resistance were obtained by using *p*-phenylenediamine as the sole precursor. These CDs exhibited sensitivity to Fe^{3+} ions, demonstrating a strong linear detection range (R^2 = 0.999) from 0 to 50 μM. Additionally, the CDs were uniform in size (2−5 nm), emitted stable red fluorescence in pH conditions ranging from 4 to 10, and were successfully internalized by glioma cells, enabling precise fluorescence imaging of gliomas both in vitro and in vivo.

1. INTRODUCTION

Glioma is a common malignant tumor of the brain that is prone to recurrence after surgery due to its highly invasive nature and poorly defined boundaries.[1] Current research shows that glioma imaging is not only useful for diagnosis but also for complete tumor removal and reducing recurrence.[2] Nanomaterials have made remarkable progress in the application of glioma imaging in recent years due to their excellent optical, magnetic, and chemical properties.[3] However, nanomaterials also have some shortcomings, such as difficulty controlling them, complex processing, and insufficient safety. Therefore, it is very important to find a new nanomaterial. Carbon nanodots (CDs), as a rising luminescent nanomaterial, have attracted extensive attention and research in recent years.[4,5] Being different from traditional quantum dots, CDs have unique optical properties with facile preparations, good biocompatibility with inexpensive starting materials, and adjustable surface functional groups with convenient postprocessing.[6−10] In addition, CDs exhibited better photostability than organic fluorescent molecules. All of these advantages promised CDs significant potential in various fields, including biomedicine, bioimaging, biosensors, optoelectronics, catalysis, and anti-counterfeiting.[11−17] In particular, CDs have shown the greatest biological applications, such as tumor imaging, due to their uniform particle sizes and negligible toxicities.[7,18]

Unfortunately, most emissions of the reported CDs were strictly dependent on the excitation light[19,20] and were thus limited to blue-green luminescence,[21,22] which severely limited their bioimaging performance due to the low tissue penetration and the strong autofluorescence of biological tissues. In comparison, red-light-emitting CDs have deep tissue penetration and negligible background interference, which are preferred in bioimaging. However, red-light emission requirements optimize the electronic band structure of CDs, which consequently often suffer from complex precursors, labor-intensive preparation, and low quantum yield.[23,24] Typically, the electronic band structure of fluorescent molecules could be

Received: June 20, 2024
Revised: October 5, 2024
Accepted: October 10, 2024
Published: October 21, 2024

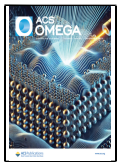

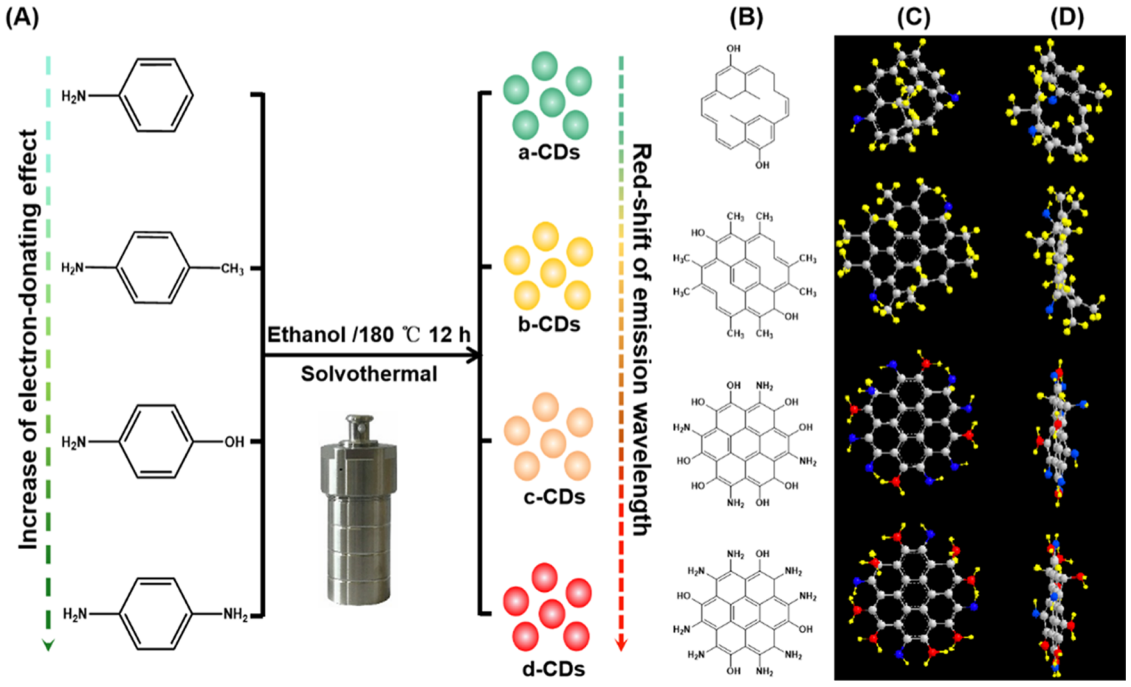

Figure 1. Illustration of the preparation of fluorescence red-shifted carbon dots (a-CDs, b-CDs, c-CDs, and d-CDs) by changing electronic effect of the synthetic precursors (A), chemical structure plane (B), 3D structural front (C) and side (D).

regulated by their surface groups, where the electron-donating effects of the surface groups can cause the emission wavelength to red shift while the electron-withdrawing effect is reversed.[25,26] However, these specific electron-donating effects on the fluorescence emission of nanoparticles (e.g., CDs) have not been determined because of the lack of appropriate preparation of different emitting CDs with similar core-surface structures.

Here, a simple solvothermal method was established to prepare fluorescent CDs with blue to red emission using four phenyl compounds (aniline, *p*-toluidine, 4-aminophenol, and *p*-phenylenediamine) with different functional groups as starting precursors. The electron-donating ability of aniline para-substituents could affect the fluorescence emission of the synthesized CDs; the stronger the electron-donating ability, the longer the emission wavelength. This provided an important theoretical reference for the subsequent design of red-emitting quantum dots. As a result, red-emitting CDs (d-CDs) with high quantum yield (~19.42%), narrow size distribution (2−5 nm), good dispersibility, and chemical stability were obtained. These d-CDs could be utilized for iron detection via Fe^{3+}-induced fluorescence quenching. More importantly, they could be taken up by the glioma cells and used for fluorescence imaging of glioma in vitro and in vivo. These findings provided a simple strategy of red-emitting CDs for robust biomedical applications.

2. MATERIALS AND METHODS

2.1. Materials. Aniline, *p*-toluidine, 4-aminophenol, and *p*-phenylenediamine were purchased from Shanghai Aladdin Bio-Chem Technology Co., Ltd. Cell lines were obtained from the Shanghai Cell Bank, Chinese Academy of Medical Sciences. The Cell counting kit-8 was purchased from Melun. Hank's solution, fetal bovine serum, and phosphate buffer saline were purchased from Hyclone. Other reagents were purchased from Gibco.

2.2. Methods. *2.2.1. Synthesis.* The CDs were prepared by the solvothermal method. First of all, *p*-phenylenediamine powder (0.9 g) was dissolved in ethanol (90 mL) and then reacted at 180 °C in an autoclave for 12 h. The solution was then naturally cooled and concentrated by using a vacuum rotary evaporator. The concentrate was then separated and purified by thin-layer chromatography. Finally, the obtained d-CDs were lyophilized for further use. As described above, the same reaction conditions and steps were used for aniline, *p*-toluidine, and 4-aminophenol.

2.2.2. Characterization. UV−vis absorption spectra, Fourier transform infrared spectroscopy (FTIR) spectra, and fluorescence spectra were obtained using a UV−vis absorption spectrometer (UV-2401PC), a Nicolet-360 FTIR spectrometer, and an FS5 fluorescence spectrophotometer (Edinburgh Instruments), respectively. Optical pictures were taken with a Canon camera. Transmission electron microscopy (TEM) images were obtained by using JEM-2010 instruments. Particle size and potential were measured by using a Malvern 3600 particle size potentiometer (U.K.). Fluorescence quantum yields (QYs) were determined and calculated according to the standard reference sample; rhodamine 6G was chosen as a standard.[27] For fluorescence stability measurements, d-CDs were dispersed in PBS at different pH values or exposed to UV light for different time periods at room temperature.

2.2.3. Cell Culture. U87MG cells (human astroblastoma cell line) were cultured in a humid incubator at 37 °C, containing 5% CO_2. The culture medium consisted of 89 wt % DMEM, 1 wt % FBS, and 1% penicillin-streptomycin. Cells were passaged when they reached 80% confluence. In general, the subculture frequency was once every 3 days.

2.2.4. Cellular Uptake. After the adherent U87MG cells or HA1800 cells were digested with trypsin, the cell pellet was obtained by centrifugation and diluted with culture medium to a concentration of 1×10^5/mL, and then the cells were seeded and allowed to grow adherently on a cell culture plate for 24 h.

https://doi.org/10.1021/acsomega.4c05770
ACS Omega 2024, 9, 44418−44424

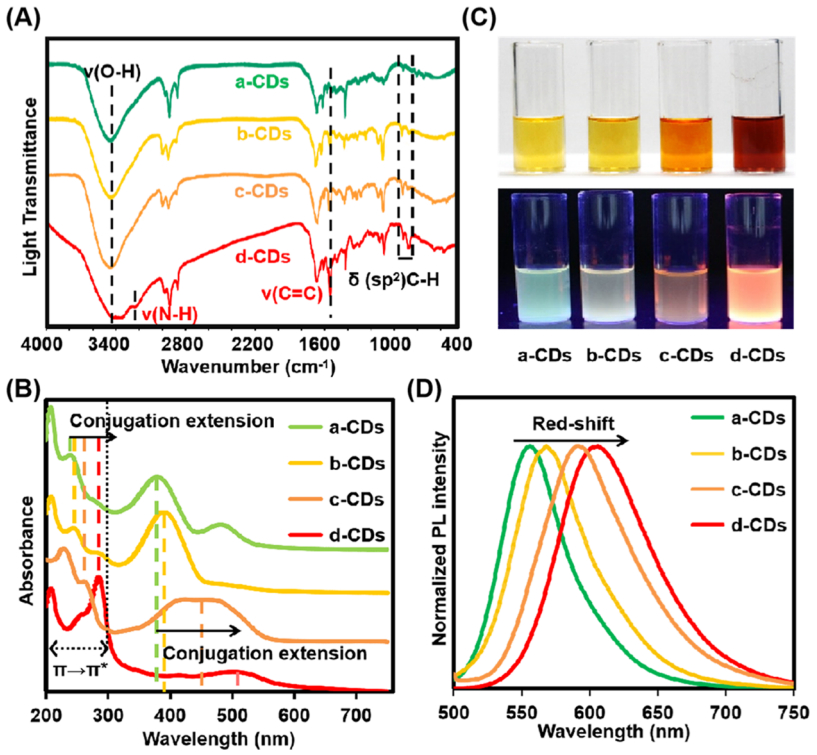

Figure 2. Characterizations of different CDs. FTIR spectra (A), UV/vis absorption spectra (B), optical images (C) under the irradiation of sunlight and UV light with a wavelength of 302 nm, and normalized PL spectra (D) (E_x = 480 nm).

The cells were then treated with d-CDs at various concentrations for 2 h. To evaluate the effect of incubation time, d-CDs (50 μg/mL) were incubated with U87MG cells for different periods of time. The cells were then washed and fixed, and the uptake of d-CDs by the cells was observed using a confocal microscope.

2.2.5. Cytotoxicity Analysis. The cytotoxicity of d-CDs was evaluated using the CCK-8 assay. U87MG cells were seeded on a 96-well plate and allowed to adhere for 24 h. The cells were then incubated with different concentrations of d-CDs for 12 h. The CCK-8 reagent was diluted with culture medium to the working concentration (10%) and added to the wells of the treated cells, incubated at 37 °C for about 1 h, and then the 96-well plate was placed in the microplate reader, and the UV absorbance of the sample at 450 nm was recorded.

2.2.6. Fluorescence Imaging. Nude mice were purchased from Shanghai SLAC Laboratory Animal Co., Ltd. U87 cells were minimally implanted into the brains of nude mice using a stereotactic fixation device (5×10^5/mice). After 19 days, 100 μL of d-CDs at a concentration of 10 mg/mL was injected (tail vein) into the nude mice. Fluorescence images were obtained with the in vivo imaging system (Caliper). The major organs of the mice were then harvested and imaged. Finally, the brain was divided into two halves and imaged again. The animal experiments were conducted according to the guidelines approved by the Ethics Committee of the First People's Hospital of Chuzhou.

3. RESULTS AND DISCUSSION

3.1. Characterizations of Four CDs. Figure 1 showed the synthesis and the proposed structures of the various CDs derived from phenyl compounds, where the electron-donating effects were reported to be $-NH_2 > -OH > -CH_3$.[28] As shown in Figure 2A, all of the CDs exhibited obvious O−H stretching vibrational absorption, suggesting the involvement of ethanol in the generation of CDs besides its service as a solvent. Moreover, all of these CDs possessed abundant surface groups. Differently, with the precursors from aniline to *p*-phenylenediamine, the obtained CDs had a gradually increased C═C stretching vibrational absorption, $C(_{SP}{}^2)$−H bending vibrational absorption, and a gradually emerged N−H stretching vibrational absorption, suggesting the elevated surface amino groups (in agreement with the precursors) and the large π-conjugation. These implied that the surface groups of the carbon dots were inherited from the precursors and that the amides favored the condensation of phenyl compounds. UV−vis absorption spectra (Figure 2B) showed that all of these carbon nanodots (a-CDs, b-CDs, c-CDs, and d-CDs) had strong absorption at 200−300 nm, which represented the π−π* transition of the aromatic C═C bond.[29] Notably, this adsorption was obviously red-shifted from 240 nm for a-CDs to 285 nm for d-CDs, indicating the most conjugated units by using phenylenediamines as precursors. Correspondingly, the maximum absorption wavelengths beyond 300 nm also behaved in this way, confirming the larger π-conjugated system for d-CDs induced by the strong electron-donating effects of the amidos in phenylenediamines.[30]

Because of their surface groups, these CDs could be dispersed in a variety of common solvents. For example, all of these CDs could be well dispersed in even ethanol solution with clear solutions of different colors (Figure 2C). In particular, these solutions could emit blue to red fluorescence under 302 nm UV light irradiation, suggesting tunable fluorescence emission. Furthermore, this distinct fluorescence could also be visualized by the normalized photoluminescence (PL) spectra (Figure 2D), which showed maximum emission wavelengths of 556, 568, 592, and 606 nm for the four carbon

https://doi.org/10.1021/acsomega.4c05770
ACS Omega 2024, 9, 44418−44424

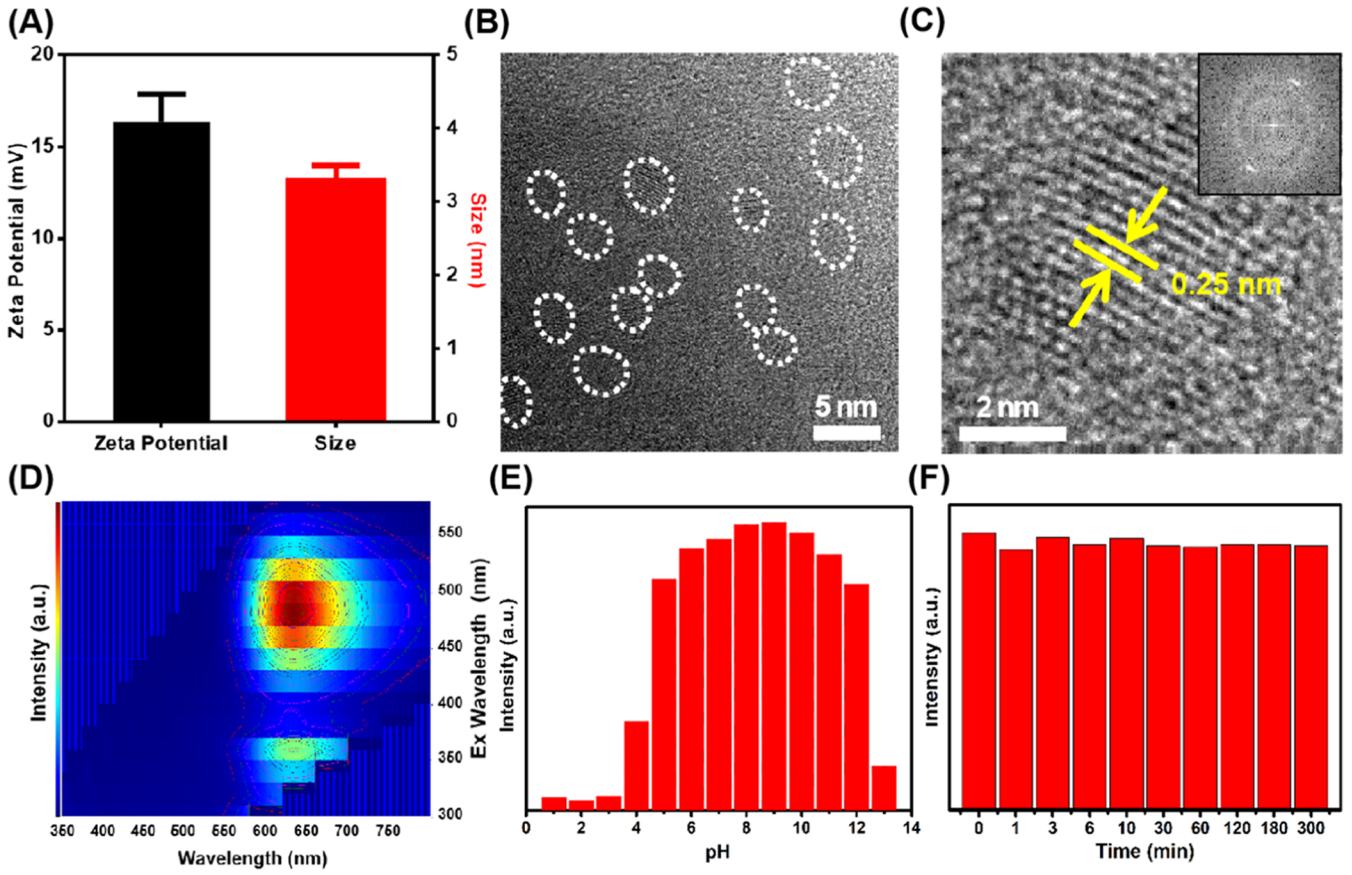

Figure 3. ζ-potential and particle size (A), TEM image (B), high-resolution TEM image (C), and Fourier transform pattern (inset of C) of d-CDs. Two-dimensional fluorescence spectrum of d-CDs (D). Fluorescence intensity of d-CDs after exposure to PBS with different pH values (E) and UV excitations with different time periods (F) (E_x = 480 nm).

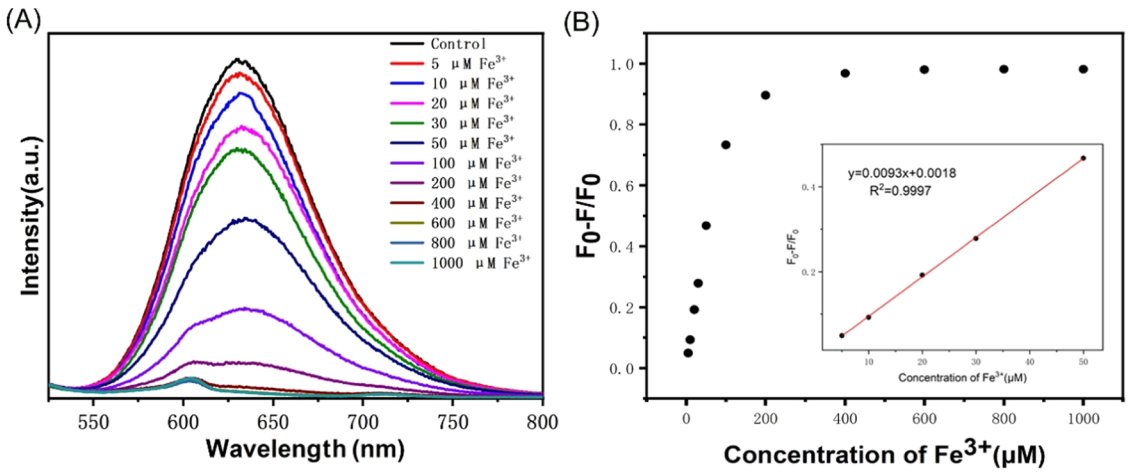

Figure 4. Fluorescence spectra (A) of d-CDs after adding different concentrations of Fe^{3+} (E_x = 480 nm) and the corresponding standard curve (B).

quantum dots, respectively. Correspondingly, the remarkable Stokes shifts of 76, 88, 112, and 126 nm indicated the easy modulation of the fluorescence emissions by the different phenyl compounds as precursors. These could be attributed to the different chemical groups ($-CH_3$, $-OH$, and $-NH_2$) in the ortho-position of the benzene rings, which could act as an electron donor for the red-shifted fluorescence according to $-CH_3 < -OH < -NH_2$.[28] Meanwhile, the $-NH_2$ facilitated the condensation reaction to form the larger conjugate structure of CDs with the reduced defects, which would also be beneficial for the red fluorescence emissions.[31] Therefore, CDs with different fluorescence emissions can be easily synthesized, and the red fluorescence CDs could be regulated for further bioapplications.

3.2. Characterizations of d-CDs. As shown in Figure 3A, the red-emitting d-CDs had a uniform ultrasmall size of about 3 nm and a ζ-potential of about 16 mV. The transmission electron microscopy (TEM) image also showed a uniform

https://doi.org/10.1021/acsomega.4c05770
ACS Omega 2024, 9, 44418−44424

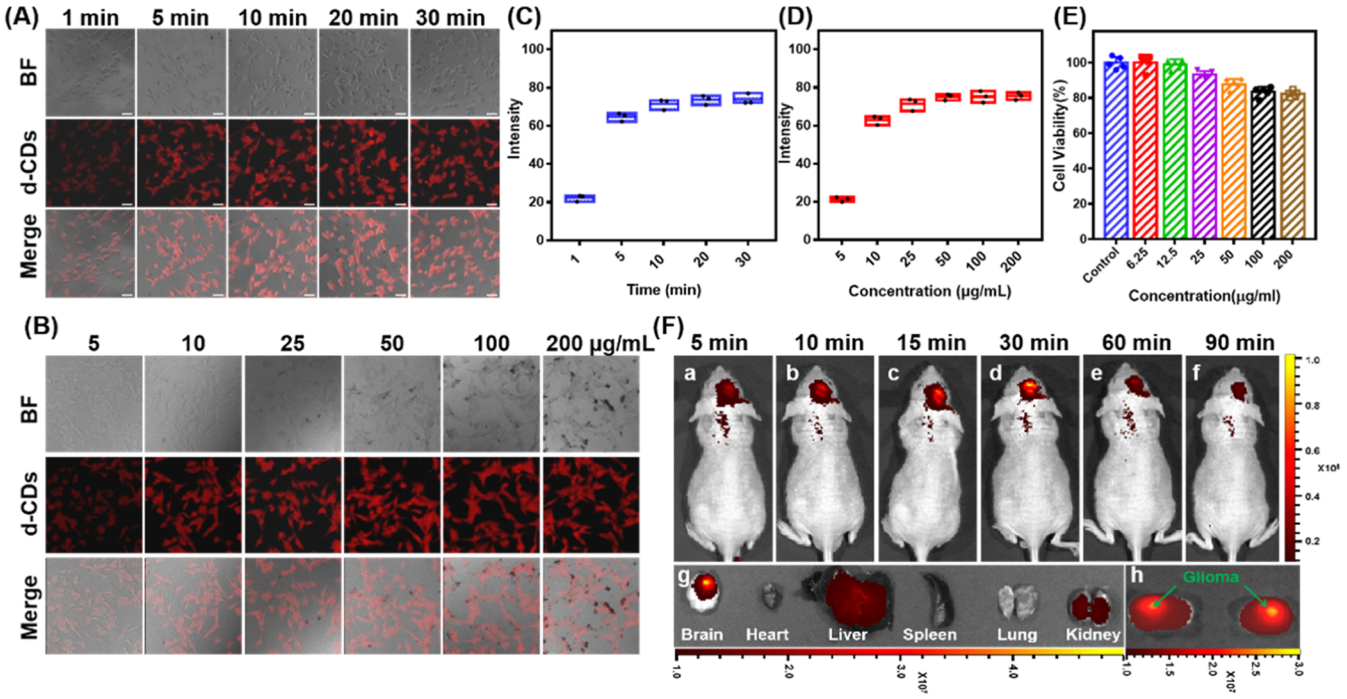

Figure 5. Cellular uptake of U87 cells cultured with d-CDs for different time periods (A, C) or different concentrations (B, D). λ_{ex} = 488 nm; bar = 50 μm. Cytotoxicity evaluated via CCK-8 test (E). Data were expressed as mean ± SD (n = 4). Fluorescence imaging images of glioma-bearing nude mice at different time points after administration (F, a−f), major organs (F, g), and the coronal plane of the brain (F, h) 30 min post injection. Data were presented as mean ± SD (n = 3).

particle size (Figure 3B). Meanwhile, a lattice spacing of 0.25 nm (Figure 2C) was observed, similar to that of graphitic carbon (100) planes, which also revealed the crystallinity of the CDs.[32] Similarly, the Fourier transform patterns (Figure 2C, inset) also confirmed the monocrystalline cores of d-CDs.[33] The optical properties of d-CDs are shown in Figure 3D. First, the emission wavelength of d-CDs was 635 nm, independent of the excitation wavelength. The optimum excitation wavelength was 480 nm. Second, the fluorescence properties of d-CDs were stable at pH 5−12 (Figure 3E) and even under a 365 nm UV irradiation time for different periods (Figure 3F). The corresponding fluorescence spectra are shown in Figure S1. Furthermore, the relative quantum yield of d-CDs was 19.42% (Figure S2). This good stability, strong photobleaching resistance, and strong fluorescence guaranteed the application of d-CDs under physiological conditions.

3.3. Biomedical Applications of d-CDs. Initially, the fluorescence of d-CDs was gradually quenched with an increasing Fe^{3+} concentration (Figure 4A). Accordingly, there was a good linear correlation relationship between the fluorescence intensity of d-CDs and the Fe^{3+} concentration (R^2 = 0.999) from 0 to 50 μM (Figure 4B). In recent years, there have been many studies on the detection of Fe^{3+} by CD, but most of them emit blue fluorescence or are used to detect abiotic substances.[34,35] Currently, the main mechanisms of Fe^{3+} detection by CD are static quenching and dynamic quenching.[36,37] Fe^{3+} has strong electron attraction and incomplete d-orbitals, so it can coordinate with functional groups (such as carboxyl, amino, or hydroxyl) on the surface of the carbon point, which leads to electron transfer, destroys the excited state energy transfer of the carbon point, and produces fluorescence quenching.[38,39] In addition, the Fe^{3+} concentration of human serum was 10−35 μM.[40] The d-CDs in this study can not only emit red light but also have a wide detection range. Therefore, it has great potential to be exploited as a chemical sensor for Fe^{3+} detection in the blood.

Next, d-CDs could be rapidly taken up by U87 glioma cells, where the maximum uptake was reached even after incubation for 10 min (Figure 5A,C). Due to the high quantum yield of 25 μg/mL d-CDs, even 10 μg/mL obviously illuminated the tumor cells via their red fluorescence (Figure 5B,D). Accordingly, d-CDs could be intravenously injected into glioma-bearing nude mice for in vivo glioma imaging (Figure 5F), where d-CDs gradually accumulated in the glioma and showed the highest brightness at 30 min after injection (a−f). Meanwhile, ex vivo fluorescence imaging of the major organs verified the targeted accumulation of d-CDs in glioma for its sensitive imaging ability (g,h in Figure 5F). In addition, d-CDs had a low cytotoxicity (Figure 5E), which was advantageous for biological applications. The above results suggested that d-CDs with good biocompatibility had great potential for glioma fluorescence imaging in vivo, which would be an advanced fluorescence contrast.

4. CONCLUSIONS

In brief, a facile solvothermal method was developed for the preparation of fluorescence CDs from blue to red emission using four phenyl compounds (aniline, *p*-toluidine, 4-aminophenol, and *p*-phenylenediamine) with different functional groups as the initial precursors. It was found that the electron-donating effects of the surface functional groups in the precursors contributed to the red shift of the emission wavelength. Consequently, red-emitting CDs (d-CDs) with high quantum yield (~19.42%), narrow size distribution (2−5 nm), good dispersibility, and strong photobleaching resistance were obtained. These d-CDs could be exploited for iron ion detection with a good linear relationship (R^2 = 0.999) from 0 μM to 50 μM via the sensitive Fe^{3+}-induced fluorescence

https://doi.org/10.1021/acsomega.4c05770
ACS Omega 2024, 9, 44418−44424

quenching. More importantly, d-CDs could be taken up by glioma cells and used for the fluorescence imaging of gliomas in vitro and in vivo. This work provided an alternative strategy and a novel insight into the preparation of CDs for further bioapplications.

■ ASSOCIATED CONTENT

Data Availability Statement

The authors confirm that the data supporting the findings of this study are available within the article and its Supporting Information.

Supporting Information

The Supporting Information is available free of charge at https://pubs.acs.org/doi/10.1021/acsomega.4c05770.

Fluorescence spectra of d-CDs and investigation of quantum yield (PDF)

■ AUTHOR INFORMATION

Corresponding Authors

Ning Lin − *Department of Neurosurgery, The Affiliated Chuzhou Hospital of Anhui Medical University, The First People's Hospital of Chuzhou, Chuzhou 239001, China*; Email: linning@ahmu.edu.cn

Yi Wang − *Center for Advanced Low-Dimension Materials, State Key Laboratory for Modification of Chemical Fibers and Polymer Materials, College of Chemistry, Chemical Engineering and Biotechnology, Donghua University, Shanghai 201600, China*; orcid.org/0000-0003-3345-4319; Email: ywang@dhu.edu.cn

Author

Shiqiang Hou − *Department of Neurosurgery, The Affiliated Chuzhou Hospital of Anhui Medical University, The First People's Hospital of Chuzhou, Chuzhou 239001, China*; orcid.org/0000-0002-5117-7442

Complete contact information is available at: https://pubs.acs.org/10.1021/acsomega.4c05770

Author Contributions

Conception and Supervision: N.L. and Y.W. Experiments and analysis of data: S.H. Preparation of the manuscript: S.H. and Y.W. Revision for important intellectual content: N.L.

Notes

The authors declare no competing financial interest.

Ethics Approval and Consent to Participate This study was approved by the Ethics Committee of the First People's Hospital of Chuzhou.

Consent for Publication All authors approved the submission to this journal.

■ ACKNOWLEDGMENTS

This work was supported by the Natural Science Foundation of Shanghai (20ZR1401800), the Scientific Research Foundation of Education Department of Anhui Province (2024AH040093, 2022AH050769, KJ2021ZD0036), and the Anhui Provincial Key Research and Development Plan (2022e07020069).

■ REFERENCES

(1) Nie, D.; Ling, Y.; Lv, W.; Liu, Q.; Deng, S.; Shi, J.; Yang, J.; Yang, Y.; Ouyang, S.; Huang, Y.; Wang, Y.; Huang, R.; Shi, W. In Situ Attached Photothermal Immunomodulation-Enhanced Nanozyme for the Inhibition of Postoperative Malignant Glioma Recurrence. *ACS Nano* **2023**, *17* (14), 13885−13902.

(2) Harat, M.; Rakowska, J.; Harat, M.; Szylberg, T.; Furtak, J.; Miechowicz, I.; Malkowski, B. Combining amino acid PET and MRI imaging increases accuracy to define malignant areas in adult glioma. *Nat. Commun.* **2023**, *14* (1), No. 4572.

(3) Zhao, W.; Yu, X.; Peng, S.; Luo, Y.; Li, J.; Lu, L. Construction of nanomaterials as contrast agents or probes for glioma imaging. *J. Nanobiotechnol.* **2021**, *19* (1), No. 125.

(4) Niranjan, R.; Prasad, G. D.; Achankunju, S.; Arockiaraj, M.; Velumani, K.; Nachimuthu, K.; Sundramoorthy, A. K.; Neogi, I.; Nallasivam, J. L.; Rajeshkumar, V.; Mahadevegowda, S. H. Multicomponent Reaction Based Tolyl-substituted and Pyrene-Pyridine Conjugated Isomeric Ratiometric Fluorescent Probes: A Comparative Investigation of Photophysical and Hg(II)-Sensing Behaviors. *J. Fluoresc.* **2023**, 1−16, DOI: 10.1007/s10895-023-03467-x.

(5) Paramasivam, G.; Palem, V. V.; Meenakshy, S.; Suresh, L. K.; Gangopadhyay, M.; Antherjanam, S.; Sundramoorthy, A. K. Advances on carbon nanomaterials and their applications in medical diagnosis and drug delivery. *Colloids Surf., B* **2024**, *241*, No. 114032.

(6) Athinarayanan, J.; Almaiman, S. A.; Al-Harbi, L. N.; Periasamy, V. S.; Alshatwi, A. A. Fabrication of fluorescent carbon nanodots from laboratory paper waste for Fe3+ ions detection. *J. King Saud Univ., Sci.* **2021**, *33* (7), No. 101584, DOI: 10.1016/j.jksus.2021.101584.

(7) Ji, D. K.; Reina, G.; Guo, S.; Eredia, M.; Samori, P.; Menard-Moyon, C.; Bianco, A. Controlled functionalization of carbon nanodots for targeted intracellular production of reactive oxygen species. *Nanoscale Horiz.* **2020**, *5* (8), 1240−1249.

(8) Lu, F.; Ma, Y.; Huang, H.; Zhang, Y.; Kong, H.; Zhao, Y.; Qu, H.; Wang, Q.; Liu, Y.; Kang, Z. Edible and highly biocompatible nanodots from natural plants for the treatment of stress gastric ulcers. *Nanoscale* **2021**, *13* (14), 6809−6818.

(9) Yang, M.-J.; Shi, J.-X.; Yin, Y.; Shi, C.-G. Preparation of Carbon Nanodots with Ultraviolet Emission by Pulsed Laser Ablation. *Phys. Status Solidi (B)* **2021**, *258* (10), No. 2100110, DOI: 10.1002/pssb.202100110.

(10) Xu, X.; Li, Y.; Hu, G.; Mo, L.; Zheng, M.; Lei, B.; Zhang, X.; Hu, C.; Zhuang, J.; Liu, Y. Surface functional carbon dots: chemical engineering applications beyond optical properties. *J. Mater. Chem. C* **2020**, *8* (46), 16282−16294.

(11) Hassanvand, Z.; Jalali, F.; Nazari, M.; Parnianchi, F.; Santoro, C. Carbon Nanodots in Electrochemical Sensors and Biosensors: A Review. *ChemElectroChem* **2021**, *8* (1), 15−35.

(12) Hu, C.; Li, M.; Qiu, J.; Sun, Y. P. Design and fabrication of carbon dots for energy conversion and storage. *Chem. Soc. Rev.* **2019**, *48* (8), 2315−2337.

(13) Khan, W. U.; Qin, L.; Alam, A.; Zhou, P.; Peng, Y.; Wang, Y. Water-soluble green-emitting carbon nanodots with enhanced thermal stability for biological applications. *Nanoscale* **2021**, *13* (7), 4301−4307.

(14) Kim, H.; Park, Y.; Beack, S.; Han, S.; Jung, D.; Cha, H. J.; Kwon, W.; Hahn, S. K. Dual-Color-Emitting Carbon Nanodots for Multicolor Bioimaging and Optogenetic Control of Ion Channels. *Adv. Sci.* **2017**, *4* (11), No. 1700325.

(15) Liu, F.; Li, Z.; Li, Y.; Feng, Y.; Feng, W. Room-temperature phosphorescent fluorine-nitrogen co-doped carbon dots: Information encryption and anti-counterfeiting. *Carbon* **2021**, *181*, 9−15.

(16) Zhang, J.; Zhang, G.; Ji, Q.; Lan, H.; Qu, J.; Liu, H. Carbon nanodot-modified FeOCl for photo-assisted Fenton reaction featuring synergistic in-situ H2O2 production and activation. *Appl. Catal., B* **2020**, *266*, No. 118665, DOI: 10.1016/j.apcatb.2020.118665.

(17) Ghosh, T.; Nandi, S.; Bhattacharyya, S. K.; Ghosh, S. K.; Mandal, M.; Banerji, P.; Das, N. C. Nitrogen and sulphur doped carbon dot: An excellent biocompatible candidate for in-vitro cancer cell imaging and beyond. *Environ. Res.* **2023**, *217*, No. 114922.

(18) Mauro, N.; Utzeri, M. A.; Drago, S. E.; Nicosia, A.; Costa, S.; Cavallaro, G.; Giammona, G. Hyaluronic acid dressing of hydrophobic carbon nanodots: A self-assembling strategy of hybrid

nanocomposites with theranostic potential. *Carbohydr. Polym.* **2021**, *267*, No. 118213.
(19) Pathak, A.; PV, S.; Stanley, J.; Babu, T. G. S. Multicolor emitting N/S-doped carbon dots as a fluorescent probe for imaging pathogenic bacteria and human buccal epithelial cells. *Mikrochim. Acta* **2019**, *186* (3), No. 157.
(20) Zheng, M.; Xie, Z. A carbon dots−based nanoprobe for intracellular Fe3+ detection. *Mater. Today Chem.* **2019**, *13*, 121−127.
(21) Yi, Z.; Li, X.; Zhang, H.; Ji, X.; Sun, W.; Yu, Y.; Liu, Y.; Huang, J.; Sarshar, Z.; Sain, M. High quantum yield photoluminescent N-doped carbon dots for switch sensing and imaging. *Talanta* **2021**, *222*, No. 121663.
(22) Zhao, D.; Zhang, R.; Liu, X.; Huang, X.; Xiao, X.; Yuan, L. One-step synthesis of blue-green luminescent carbon dots by a low-temperature rapid method and their high-performance antibacterial effect and bacterial imaging. *Nanotechnology* **2021**, *32* (15), No. 155101.
(23) Holá, K.; Sudolska, M.; Kalytchuk, S.; Nachtigallova, D.; Rogach, A. L.; Otyepka, M.; Zboril, R. Graphitic Nitrogen Triggers Red Fluorescence in Carbon Dots. *ACS Nano* **2017**, *11* (12), 12402−12410.
(24) Liu, Y.; Duan, W.; Song, W.; Liu, J.; Ren, C.; Wu, J.; Liu, D.; Chen, H. Red Emission B, N, S-co-Doped Carbon Dots for Colorimetric and Fluorescent Dual Mode Detection of Fe(3+) Ions in Complex Biological Fluids and Living Cells. *ACS Appl. Mater. Interfaces* **2017**, *9* (14), 12663−12672.
(25) Sun, Z.; Jiang, Y.; Zeng, L.; Zhang, X.; Hu, S.; Huang, L. Controllable local electronic migration induced charge separation and red-shift emission in carbon nitride for enhanced photocatalysis and potential phototherapy. *Chem. Commun.* **2019**, *55* (43), 6002−6005.
(26) Xin, G.; Wang, H.; Kim, N.; Hwang, W.; Cho, S. M.; Chae, H. Investigation of charge-transfer complexes formation between photo-luminescent graphene oxide and organic molecules. *Nanoscale* **2012**, *4* (2), 405−407.
(27) Feng, X. T.; Zhang, F.; Wang, Y. L.; Zhang, Y.; Yang, Y. Z.; Liu, X. G. Luminescent carbon quantum dots with high quantum yield as a single white converter for white light emitting diodes. *Appl. Phys. Lett.* **2015**, *107* (21), No. 213102, DOI: 10.1063/1.4936234.
(28) Yuan, X.; Wang, W.; Tian, Z.; Bi, S.; Ma, J. Electron-donating groups and high ring strain promoted ring opening of methylenecyclopropanes catalyzed by rhodium and iridium complexes. *J. Organomet. Chem.* **2016**, *811*, 29−39.
(29) Hua, X. W.; Bao, Y. W.; Zeng, J.; Wu, F. G. Nucleolus-Targeted Red Emissive Carbon Dots with Polarity-Sensitive and Excitation-Independent Fluorescence Emission: High-Resolution Cell Imaging and in Vivo Tracking. *ACS Appl. Mater. Interfaces* **2019**, *11* (36), 32647−32658.
(30) Lash, T. D.; Chandrasekar, P. Synthesis of tetraphenyltetraacenaphthoporphyrin: A new highly conjugated porphyrin system with remarkably red-shifted electronic absorption spectra. *J. Am. Chem. Soc.* **1996**, *118*, 8767−8768.
(31) Qu, S.; Zhou, D.; Li, D.; Ji, W.; Jing, P.; Han, D.; Liu, L.; Zeng, H.; Shen, D. Toward Efficient Orange Emissive Carbon Nanodots through Conjugated sp(2) -Domain Controlling and Surface Charges Engineering. *Adv. Mater.* **2016**, *28* (18), 3516−3521.
(32) Deng, X.; Feng, Y.; Li, H.; Du, Z.; Teng, Q.; Wang, H. N-doped carbon quantum dots as fluorescent probes for highly selective and sensitive detection of Fe3+ ions. *Particuology* **2018**, *41*, 94−100.
(33) Tang, J.; Kong, B.; Wu, H.; Xu, M.; Wang, Y.; Wang, Y.; Zhao, D.; Zheng, G. Carbon nanodots featuring efficient FRET for real-time monitoring of drug delivery and two-photon imaging. *Adv. Mater.* **2013**, *25* (45), 6569−6574.
(34) Atchudan, R.; Edison, T.; Aseer, K. R.; Perumal, S.; Karthik, N.; Lee, Y. R. Highly fluorescent nitrogen-doped carbon dots derived from Phyllanthus acidus utilized as a fluorescent probe for label-free selective detection of Fe(3+) ions, live cell imaging and fluorescent ink. *Biosens. Bioelectron.* **2018**, *99*, 303−311.
(35) Nagaraj, M.; Ramalingam, S.; Murugan, C.; Aldawood, S.; Jin, J. O.; Choi, I.; Kim, M. Detection of Fe(3+) ions in aqueous environment using fluorescent carbon quantum dots synthesized from endosperm of Borassus flabellifer. *Environ. Res.* **2022**, *212* (Pt B), No. 113273.
(36) Naresh, V.; Lee, N. A Review on Biosensors and Recent Development of Nanostructured Materials-Enabled Biosensors. *Sensors* **2021**, *21* (4), No. 1109, DOI: 10.3390/s21041109.
(37) Qi, H.; Teng, M.; Liu, M.; Liu, S.; Li, J.; Yu, H.; Teng, C.; Huang, Z.; Liu, H.; Shao, Q.; Umar, A.; Ding, T.; Gao, Q.; Guo, Z. Biomass-derived nitrogen-doped carbon quantum dots: highly selective fluorescent probe for detecting Fe(3+) ions and tetracyclines. *J. Colloid Interface Sci.* **2019**, *539*, 332−341.
(38) Sushma; Sharma, S. S.; Ghosh, K. S. Applications of Functionalized Carbon-Based Quantum Dots in Fluorescence Sensing of Iron(III). *J. Fluoresc.* **2024**, 1−18, DOI: 10.1007/s10895-024-03611-1.
(39) Zhou, Y.; Chen, G.; Ma, C.; Gu, J.; Yang, T.; Li, L.; Gao, H.; Xiong, Y.; Wu, Y.; Zhu, C.; Wu, H.; Yin, W.; Hu, A.; Qiu, X.; Guan, W.; Zhang, W. Nitrogen-doped carbon dots with bright fluorescence for highly sensitive detection of Fe(3+) in environmental waters. *Spectrochim. Acta, Part A* **2023**, *293*, No. 122414.
(40) Kuo, C.-T.; Lin, C.-H.; Lii, Y.-A.; Gu, M.-W.; Pao, C.-W.; Lee, J.-F.; Chen, C.-h. Quantification signalling via transition of solution inhomogeneity: determination of iron content in human serum by the naked eye. *Anal. Methods* **2014**, *6* (18), 7204−7211.

https://doi.org/10.1021/acsomega.4c05770
ACS Omega 2024, 9, 44418−44424